

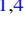







Parallel-propagating Fluctuations at Proton-kinetic Scales in the Solar Wind Are Dominated By Kinetic Instabilities

Lloyd D. Woodham^{1,2} , Robert T. Wicks^{1,3} , Daniel Verscharen^{1,4} , Christopher J. Owen¹ , Bennett A. Maruca^{5,6} , and Benjamin L. Alterman^{7,8} 

¹ Mullard Space Science Laboratory, University College London, Holmbury St. Mary, Surrey RH5 6NT, UK; woodhamlloyd@gmail.com

² Department of Physics, The Blackett Laboratory, Imperial College London, London SW7 2AZ, UK

³ Institute of Risk and Disaster Reduction, University College London, London WC1E 6BT, UK

⁴ Space Science Center, University of New Hampshire, Durham, NH 03824, USA

⁵ Department of Physics and Astronomy, University of Delaware, Newark, DE 19716, USA

⁶ Bartol Research Institute, University of Delaware, Newark, DE 19716, USA

⁷ Department of Climate and Space Sciences and Engineering, University of Michigan, Ann Arbor, MI 48109, USA

⁸ Department of Applied Physics, University of Michigan, Ann Arbor, MI 48109, USA

Received 2019 August 20; revised 2019 October 3; accepted 2019 October 4; published 2019 October 18

Abstract

We use magnetic helicity to characterize solar wind fluctuations at proton-kinetic scales from *Wind* observations. For the first time, we separate the contributions to helicity from fluctuations propagating at angles quasi-parallel and oblique to the local mean magnetic field, \mathbf{B}_0 . We find that the helicity of quasi-parallel fluctuations is consistent with Alfvén-ion cyclotron and fast magnetosonic-whistler modes driven by proton temperature anisotropy instabilities and the presence of a relative drift between α -particles and protons. We also find that the helicity of oblique fluctuations has little dependence on proton temperature anisotropy and is consistent with fluctuations from the anisotropic turbulent cascade. Our results show that parallel-propagating fluctuations at proton-kinetic scales in the solar wind are dominated by proton temperature anisotropy instabilities and not the turbulent cascade. We also provide evidence that the behavior of fluctuations at these scales is independent of the origin and macroscopic properties of the solar wind.

Unified Astronomy Thesaurus concepts: [Space plasmas \(1544\)](#); [Plasma astrophysics \(1261\)](#); [Plasma physics \(2089\)](#); [Solar wind \(1534\)](#); [Heliosphere \(711\)](#); [Interplanetary turbulence \(830\)](#); [Alfvén waves \(23\)](#); [Slow solar wind \(1873\)](#); [Fast solar wind \(1872\)](#)

1. Introduction

The solar wind is a plasma that emanates from the solar corona and expands supersonically to form the heliosphere. This dynamic environment supports fluctuations such as turbulence, waves, and instabilities over a broad range of scales (Verscharen et al. 2019). The coupling of electromagnetic fluctuations and particles over many scales is integral to energy transport and heating in plasmas. In situ measurements of the solar wind provide insights into these fundamental processes, making it a unique plasma laboratory to better understand other astrophysical plasmas that are inaccessible to spacecraft.

Solar wind fluctuations are predominately Alfvénic and exhibit a turbulent cascade of energy from large to small scales that is mediated by nonlinear interactions (Bruno & Carbone 2013; Chen 2016). At wave numbers $k \ll 2\pi/d_p$ and $k \ll 2\pi/\rho_p$, where d_p is the proton inertial length and ρ_p is the proton gyroradius, the plasma behaves as a fluid. This range of scales is denoted the inertial range of turbulence and is characterized by fluctuations with increasing anisotropy ($k_\perp \gg k_\parallel$) towards smaller scales with respect to \mathbf{B}_0 , the local mean magnetic field (Wicks et al. 2010; Chen et al. 2011, 2012; Horbury et al. 2012; Lacombe et al. 2017). At proton-kinetic scales, i.e., $k \sim 2\pi/d_p$ and $k \sim 2\pi/\rho_p$, Hall and Larmor-radius effects become important in mediating the physics of the cascade (Alexandrova et al. 2013), and the Alfvénic fluctuations show properties consistent with dispersive kinetic Alfvén waves (KAWs; Leamon et al. 1999; Bale et al. 2005; Howes et al. 2008; Sahraoui et al. 2010). At these scales, the turbulent

fluctuations are prone to collisionless damping via wave-particle interactions, which leads to fine structure in particle velocity distribution functions (VDFs; Chen et al. 2019). This fine structure increases the effective collision rate, enabling dissipation of the fluctuations and leading to plasma heating.

Solar wind particle VDFs often deviate from isotropic Maxwellian distributions due to a low rate of collisional relaxation (Kasper et al. 2008; Marsch 2012; Maruca et al. 2013; Kasper et al. 2017). Non-Maxwellian features such as temperature anisotropies relative to \mathbf{B}_0 , beams, and relative drifts between plasma species provide sources of free energy for instabilities (Kasper et al. 2002; Hellinger et al. 2006; Kasper et al. 2008; Bale et al. 2009; Maruca et al. 2012; Bourouaine et al. 2013; Kasper et al. 2013; Gary et al. 2015; Alterman et al. 2018). One example is the proton temperature anisotropy, $T_{p,\perp}/T_{p,\parallel}$, where $T_{p,\perp}$ and $T_{p,\parallel}$ are the proton temperatures perpendicular and parallel to \mathbf{B}_0 , respectively. As the solar wind flows out into the heliosphere, local processes drive changes in $T_{p,\perp}/T_{p,\parallel}$, leading to a deviation from Chew–Goldberger–Low theory for adiabatic expansion (Chew et al. 1956; Matteini et al. 2007). If $T_{p,\perp}/T_{p,\parallel}$ deviates far enough from unity, kinetic instabilities grow that act to limit this anisotropy. Measurements of the near-Earth solar wind show that the observed range of $T_{p,\perp}/T_{p,\parallel}$ values is constrained by the increasing growth rates of these anisotropy-driven instabilities (Kasper et al. 2002; Hellinger et al. 2006; Bale et al. 2009; Maruca et al. 2012). In fact, Klein et al. (2018) show that over half of solar wind intervals support ion-scale kinetic instabilities, suggesting that they are ubiquitous in the solar wind.

Four kinetic instabilities driven by proton temperature anisotropy are relevant in the solar wind. The Alfvén ion-cyclotron (AIC) and mirror-mode instabilities are unstable at $T_{p,\perp}$ sufficiently greater than $T_{p,\parallel}$. On the other hand, the parallel and oblique firehose instabilities are unstable at $T_{p,\parallel}$ sufficiently greater than $T_{p,\perp}$. The AIC and parallel firehose instabilities have maximum growth rates for wave vectors, \mathbf{k} , that are parallel to \mathbf{B}_0 , which respectively leads to growing AIC and fast magnetosonic-whistler (FMW) modes at $k_{\parallel}d_p \lesssim 1$. Conversely, the mirror-mode and oblique firehose instabilities, have maximum growth rates for \mathbf{k} at angles oblique to \mathbf{B}_0 , and drive modes at $k_{\perp}\rho_p \lesssim 1$ that do not propagate in the plasma frame. The two parallel instabilities can also be driven unstable by particle beams and drifts (Bourouaine et al. 2013; Verscharen et al. 2013), for example, the differential flow between α -particles and protons, $\mathbf{v}_d = \mathbf{v}_{\alpha} - \mathbf{v}_p$ (Neugebauer et al. 1994, 1996; Steinberg et al. 1996). This drift velocity is about $v_d \simeq 0.6 v_A$, where v_A the local Alfvén speed, and directed along \mathbf{B}_0 away from the Sun (Kasper et al. 2006; Alterman et al. 2018). Podesta & Gary (2011a, 2011b) show that the presence of a differential flow leads to a preferential driving of the AIC and parallel firehose instabilities in the direction of \mathbf{v}_d and $-\mathbf{v}_d$, respectively.

Several studies (He et al. 2011, 2012a, 2012b; Podesta & Gary 2011b; Klein et al. 2014; Bruno & Telloni 2015; Telloni et al. 2015) use magnetic helicity to characterize solar wind fluctuations at proton-kinetic scales. However, Taylor’s hypothesis (Taylor 1938) limits single-spacecraft observations to the spacecraft frame, so that we can only measure a projection of \mathbf{k} along the flow direction past the spacecraft, $k_r = \mathbf{k} \cdot \mathbf{v}_{sw}$, where \mathbf{v}_{sw} is the solar wind velocity. In this Letter, we use a novel method to measure the wave-vector anisotropy of solar wind magnetic field fluctuations using magnetic helicity (Wicks et al. 2012). For the first time, we separate the helicity of fluctuations propagating at quasi-parallel and oblique angles to \mathbf{B}_0 . We find that periods of strong coherent helicity correspond to parallel-propagating fluctuations during intervals in which the plasma is unstable due to its proton temperature anisotropy. These fluctuations are preferentially driven due to the presence of a significant drift between α -particles and protons. Furthermore, we show that the continual background helicity in the solar wind corresponds to fluctuations propagating oblique to \mathbf{B}_0 . The amplitude of this signature shows little dependence on $\beta_{p,\parallel}$ and $T_{p,\perp}/T_{p,\parallel}$, and we attribute these fluctuations to the anisotropic turbulent cascade (Horbury et al. 2008; Chen et al. 2010; Wicks et al. 2010). Our results suggest there is no strong parallel component of the turbulent cascade at proton-kinetic scales.

2. Magnetic Helicity

Magnetic helicity is a measure of the phase coherence between magnetic field components and serves as a useful indicator of the polarization properties of solar wind fluctuations. The fluctuating magnetic helicity density in spectral form is defined as $H_m(\mathbf{k}) \equiv \mathbf{A}(\mathbf{k}) \cdot \mathbf{B}^*(\mathbf{k})$, where \mathbf{A} is the fluctuating magnetic vector potential, \mathbf{B} is the fluctuating magnetic field, and the asterisk indicates the complex conjugate of the Fourier coefficients (Matthaeus & Goldstein 1982). From a single-spacecraft time series of magnetic field measurements, we can only determine a reduced form of the magnetic helicity density (Batchelor 1970; Montgomery & Turner 1981; Matthaeus et al.

1982):

$$H_m^r(k_r) = \frac{2 \operatorname{Im} \{P_{TN}(k_r)\}}{k_r}, \quad (1)$$

where $P_{ij}(k_r) = B_i^*(k_r) \cdot B_j(k_r)$ is the reduced power spectral tensor in RTN coordinates. We define the normalized reduced fluctuating magnetic helicity density as:

$$\sigma_m(k_r) \equiv \frac{k_r H_m^r(k_r)}{|\mathbf{B}(k_r)|^2} = \frac{2 \operatorname{Im} \{P_{TN}(k_r)\}}{\operatorname{Tr} \{P(k_r)\}}, \quad (2)$$

where $\operatorname{Tr}\{\}$ denotes the trace. Here, $\sigma_m(k_r)$ is dimensionless and takes values between $[-1, 1]$, where $\sigma_m = -1$ indicates purely left-handed and $\sigma_m = +1$ indicates purely right-handed circular fluctuations, respectively. A value of $\sigma_m = 0$ indicates no overall coherence. We define the field-aligned coordinate system $(\hat{x}, \hat{y}, \hat{z})$,

$$\hat{z} = \frac{\mathbf{B}_0}{|\mathbf{B}_0|}; \hat{y} = -\frac{\mathbf{v}_{sw} \times \mathbf{B}_0}{|\mathbf{v}_{sw} \times \mathbf{B}_0|}; \hat{x} = \hat{y} \times \hat{z}, \quad (3)$$

so that \mathbf{v}_{sw} lies in the \hat{x} - \hat{z} plane (Wicks et al. 2012). This coordinate system exploits Taylor’s hypothesis so that we can separate the different contributions to magnetic helicity from fluctuations propagating quasi-parallel and oblique to \mathbf{B}_0 using the definition:

$$\sigma_{ij}(k_r) = \frac{2 \operatorname{Im} \{P_{ij}(k_r)\}}{\operatorname{Tr} \{P(k_r)\}}, \quad (4)$$

where the indices $i, j = x, y, z$. Therefore, σ_{xy} gives the helicity of fluctuations with $\mathbf{k} \times \mathbf{B}_0 \simeq 0$ and σ_{xy} the helicity for fluctuations with $\mathbf{k} \times \mathbf{B}_0 \neq 0$. The component σ_{xz} integrates to zero if the distribution of fluctuation power is gyrotropic. This novel analysis technique allows us to recover additional information about the wave-vector of the fluctuations using magnetic helicity, without assuming any particular linear or nonlinear wave mode.

3. Method

We analyze magnetic field and ion moment data from the MFI fluxgate magnetometer (Lepping et al. 1995; Koval & Szabo 2013) and SWE Faraday cup (Ogilvie et al. 1995; Kasper et al. 2006) instruments on board the *Wind* spacecraft (Acuña et al. 1995) from 2004 June to 2018 October. We neglect collisionally old wind, $A_c \geq 1$, where A_c is the collisional age (Maruca et al. 2013), which estimates the number of collisional timescales for protons. To account for heliospheric sector structure in the magnetic field measurements, we first calculate the Parker-spiral angle, $\theta_{rB} = \arctan(B_{0,T}/B_{0,R})$, where $B_{0,R}$ and $B_{0,T}$ are the average components of \mathbf{B}_0 over 92 s periods. If $\langle \theta_{rB} \rangle$ over a two day period exceeds 45° from the radial direction, we reverse the signs of the $B_{0,R}$ and $B_{0,T}$ components so that inwards fields are rotated outwards. This procedure removes the inversion of the sign of magnetic helicity due to the direction \mathbf{B}_0 with respect to the Sun.

We transform the 11 Hz magnetic field data into field-aligned coordinates (Equation (3)) using \mathbf{B}_0 averaged over 92 s. We compute the continuous wavelet transform (Torrence & Compo 1998) using a Morlet wavelet to obtain $P(f)$ as a function of the spacecraft-frame frequency, $f = k_r |\mathbf{v}_{sw}| / 2\pi$.

Table 1The Four Cases for $\mathbf{k} \cdot \mathbf{B}_0$ in the Solar Wind Due to Sector Structure

	I	II	III	IV
\mathbf{B}_0	Out	Out	In	In
\mathbf{k}	Out	In	Out	In
σ_L^a	–	+	+	–
σ_R	+	–	–	+

Note.

^a Here, σ_L and σ_R give the sign of the magnetic helicity due to left-handed and right-handed fluctuations, respectively. The +(–) sign designates a positive (negative) helicity.

We then calculate magnetic helicity spectra, σ_{xy} and σ_{xy} , using Equation (4). We average the spectra over 92 s so that a single spectrum overlaps with exactly one SWE measurement, giving a total of 1,696,270 observations, excluding data gaps. This averaging ensures that fluctuations persist for at least several proton gyro-periods, $2\pi/\Omega_p$, to give a clear coherent helicity signature at proton-kinetic scales. Following Woodham et al. (2018), we estimate the amplitude of σ_{xy} and σ_{xy} at proton-kinetic scales by fitting a Gaussian to the coherent peak in each spectrum at frequencies $f \sim 0.8$ Hz, close to the Taylor-shifted frequencies for d_p and ρ_p . We neglect any peak at $f > f_{\text{noise}}$, the frequency at which instrumental noise of the MFI magnetometer becomes significant.⁹ We also reject a spectrum if the angular deviation in \mathbf{B} exceeds 15° during the measurement period to ensure that fluctuations at proton-kinetic scales retain their anisotropy with respect to \mathbf{B}_0 over 92 s. We designate the amplitude of the peak in each σ_{xy} and σ_{xy} spectrum as σ_{\parallel} and σ_{\perp} , respectively.

We bin σ_{\parallel} and σ_{\perp} in $\beta_{p,\parallel} - T_{p,\perp}/T_{p,\parallel}$ space using logarithmic bins, where $\beta_{p,\parallel} = n_p k_B T_{p,\parallel} / (B_0^2 / 2\mu_0)$, n_p is the proton density and $B_0 = |\mathbf{B}_0|$. We use equal bin widths of $\Delta \log_{10}(\beta_{p,\parallel}) = \Delta \log_{10}(T_{p,\perp}/T_{p,\parallel}) = 0.05$ and restrict our analysis to $0.01 \leq \beta_{p,\parallel} \leq 10$ and $0.1 \leq T_{p,\perp}/T_{p,\parallel} \leq 10$. In our plots, we neglect any bins with fewer than 10 data points to increase the likelihood of statistical convergence. In this parameter space we overplot contours of constant maximum growth rate, γ/Ω_p , for the four kinetic instabilities driven by proton temperature anisotropy. We calculate these contours using linear Vlasov–Maxwell theory (see Maruca et al. 2012 and references therein).

4. Results and Discussion

The presence of an α -particle drift can break the symmetry of the proton VDFs, leading to a preferential driving of waves generated by anisotropy-driven AIC and parallel firehose instabilities. Linear Vlasov–Maxwell theory shows that the growth rates of AIC and FMW modes are greater in the anti-sunward and sunward directions, respectively, for \mathbf{v}_d directed anti-sunward (Podesta & Gary 2011a, 2011b). The propagation of AIC and FMW modes in different directions therefore leads to sign changes in the helicity of these waves when σ_{\parallel} is transformed from the plasma-frame to the spacecraft-frame. We summarize the possible cases for the sign of σ_{\parallel} in Table 1. For example, if \mathbf{B}_0 is directed anti-sunward, then left-handed AIC modes will have $\sigma_{\parallel} < 0$ or $\sigma_{\parallel} > 0$ if they propagate anti-

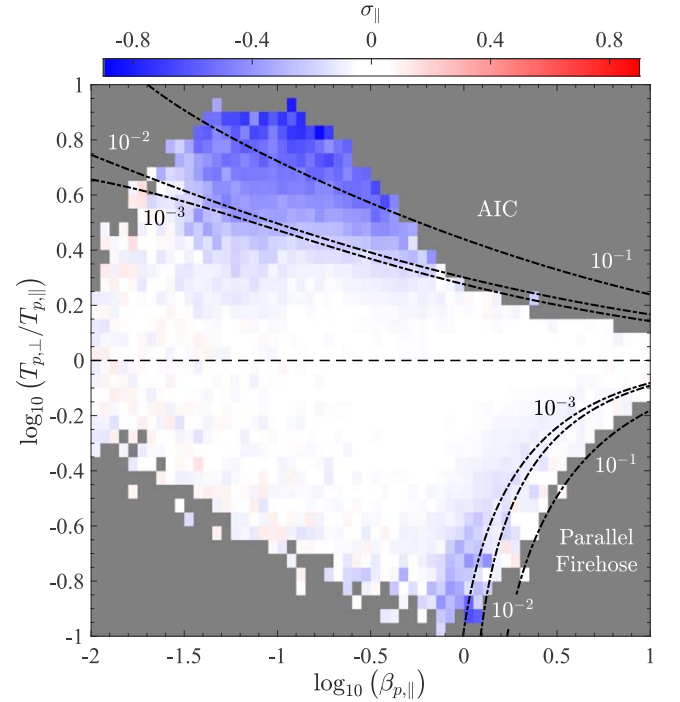


Figure 1. Median value of σ_{\parallel} across $\beta_{p,\parallel} - T_{p,\perp}/T_{p,\parallel}$ space. We overplot contours of different constant maximum growth rates, γ/Ω_p , for the AIC and parallel firehose instabilities.

sunward or sunward, respectively. By accounting for sector structure (see Section 3), our resulting data set is consistent with either case I or II from Table 1, removing ambiguity in the sign of σ_{\parallel} due to the direction of \mathbf{B}_0 . Therefore, we hypothesize that $\sigma_{\parallel} < 0$ for both AIC and FMW modes present at proton-kinetic scales in the solar wind.

To test this hypothesis, we plot in Figure 1 the median σ_{\parallel} -value across the $\beta_{p,\parallel} - T_{p,\perp}/T_{p,\parallel}$ plane. The black dashed lines show contours of constant γ/Ω_p for the AIC and parallel firehose instabilities, which have greater growth rates along \mathbf{B}_0 . We see that the solar wind plasma occupies a significant extent of parameter space in the regions unstable to both the AIC and parallel firehose instabilities, as widely reported in the literature (e.g., Hellinger et al. 2006; Bale et al. 2009; Maruca et al. 2012). In these regions of parameter space, we see two distinct signatures at $T_{p,\perp} > T_{p,\parallel}$ and $T_{p,\perp} < T_{p,\parallel}$ where the median value of σ_{\parallel} assumes more negative values. These signatures indicate the presence of coherent fluctuations that we attribute to growing modes from these instabilities. The minimum helicity is about $\sigma_{\parallel} \simeq -0.6$ for the AIC modes and $\sigma_{\parallel} \simeq -0.4$ for the FMW modes. Since $\sigma_{\parallel} < 0$ corresponds to left-handed helicity in the spacecraft frame, Figure 1 indicates that AIC modes are preferentially driven anti-sunward, and that FMW modes are preferentially driven sunward. We confirm that these fluctuations have median $k_{\parallel} d_p \sim 1$ at the peak value of σ_{\parallel} from Figure 1 (not shown here), in agreement with the predictions for linear growth of AIC and FMW modes (e.g., see Klein & Howes 2015). This result is consistent with our predictions as well as observations of quasi-parallel propagating waves in the solar wind (Tsurutani et al. 1994; Jian et al. 2009, 2010; He et al. 2011, 2012a, 2012b, 2015; Podesta & Gary 2011b; Jian et al. 2014; Klein et al. 2014; Bruno & Telloni 2015; Telloni et al. 2015; Telloni & Bruno 2016; Wicks et al. 2016; Zhao et al. 2018, 2019). Away from the unstable regions of the

⁹ See the Appendix in Woodham et al. (2018).

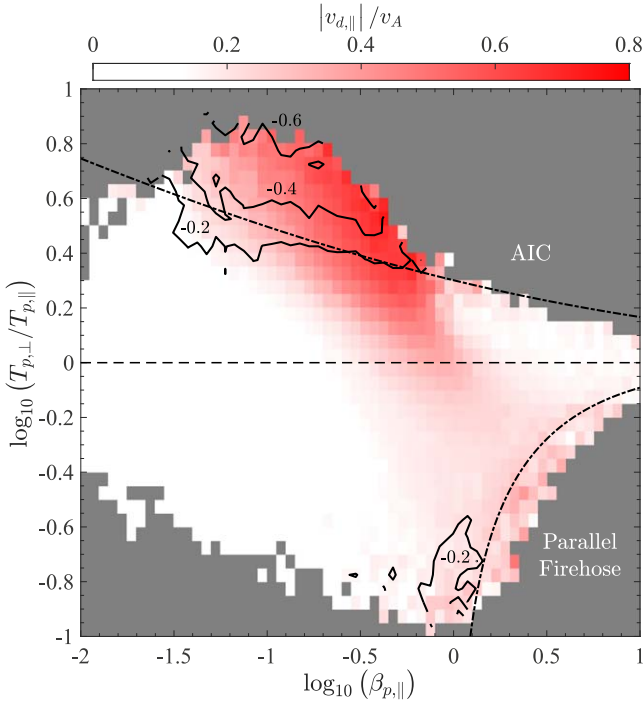


Figure 2. Median parallel α -proton drift, $|v_{d,||}|/v_A$, across $\beta_{p,||} - T_{p,\perp}/T_{p,||}$ space. We overplot contours of constant maximum growth rate, $\gamma/\Omega_p = 10^{-2}$, for the AIC and parallel firehose instabilities. We also show contours of constant $\sigma_{||}$ from Figure 1 for reference.

parallel instabilities in parameter space and close to $T_{p,\perp} \simeq T_{p,||}$, $\sigma_{||} \simeq 0$, which indicates a lack of coherence in \mathbf{B} .

In Figure 2, we plot the median value of $|v_{d,||}|/v_A$, the α -particle parallel drift speed normalized by the Alfvén speed, across the $\beta_{p,||} - T_{p,\perp}/T_{p,||}$ plane. We define $v_{d,||} = \mathbf{v}_d \cdot \mathbf{B}_0/|\mathbf{B}_0|$. We include contours of constant $\sigma_{||}$ from Figure 1 to show the correlation between $|v_{d,||}|/v_A$ and $\sigma_{||}$ in this space. When a significant drift exists close to the unstable regions of the AIC and parallel firehose instabilities, a coherent signature in $\sigma_{||}$ also exists. The drift is stronger for $T_{p,\perp}/T_{p,||} > 1$, reaching a maximum of $|v_{d,||}| \simeq 0.6 v_A$ at $\beta_{p,||} > 0.1$. This peak in $|v_{d,||}|$ occurs in the region of parameter space dominated by fast wind streams (Matteini et al. 2007). For parallel firehose unstable regions of the parameter space, the drift is significantly weaker, reaching a maximum of $|v_{d,||}| \simeq 0.2 v_A$. Therefore, the presence of a drift between ion species in the solar wind can explain the preferential driving associated with the AIC and FMW modes, which is consistent with previous studies (Podesta & Gary 2011a; Verscharen et al. 2013; Klein et al. 2018).

Finally, in Figure 3 we plot the median σ_{\perp} -value in the same parameter space. We include contours of constant γ/Ω_p for the mirror-mode and oblique firehose instabilities since these have higher growth rates at angles oblique to \mathbf{B}_0 . Throughout Figure 3, $\sigma_{\perp} > 0$ and peaks at $\sigma_{\perp} \simeq 0.3$, close to $\beta_{p,||} \simeq 0.8$ and $T_{p,\perp} \sim T_{p,||}$. This peak lies in a region of parameter space dominated by fast wind, which is typically more Alfvénic (Stansby et al. 2019). There is also a small enhancement in the helicity in the unstable region of the oblique firehose instability, suggesting the presence of driven modes with a right-handed helicity in the spacecraft-frame. We do not expect to observe a signature from mirror-modes because they represent structures with \mathbf{B} directed along \mathbf{B}_0 , which will not be measurable using magnetic helicity.

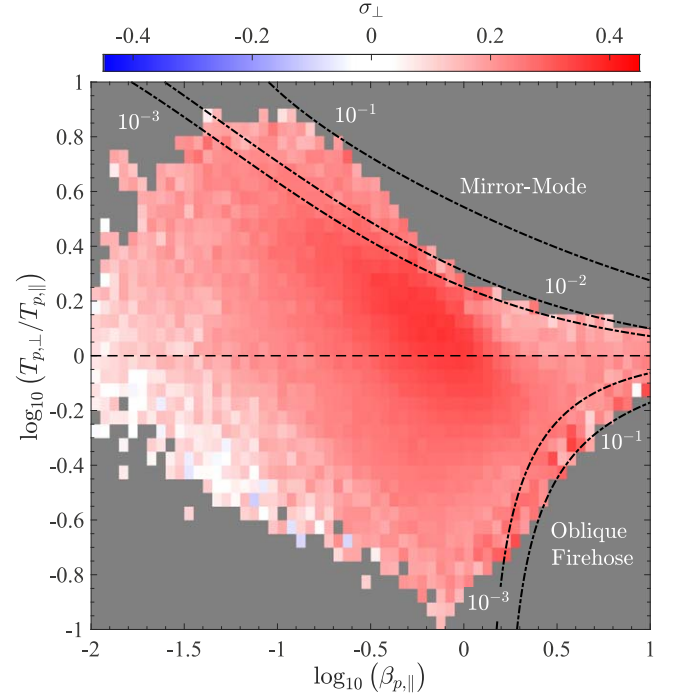


Figure 3. Median value of σ_{\perp} across $\beta_{p,||} - T_{p,\perp}/T_{p,||}$ space. We overplot contours of different constant maximum growth rates, γ/Ω_p , for the mirror-mode and oblique firehose instabilities.

The lack of a strong dependence of the distribution of σ_{\perp} on $\beta_{p,||}$ and $T_{p,\perp}/T_{p,||}$ implies that the dominant source of these fluctuations is unlikely to be related to kinetic instabilities. Instead, due to the anisotropic nature of the turbulent cascade at proton-kinetic scales, we expect turbulent fluctuations to contribute to σ_{\perp} due to the mode conversion of Alfvénic to KAW-like fluctuations at these scales (Markovskii et al. 2015). From linear Vlasov–Maxwell theory, right-handed KAWs with $k_{\perp} \gg k_{||}$ at kinetic scales ($k_{\perp} \rho_p \gtrsim 1$) have $\sigma_{\perp} \simeq 1$ for $\mathbf{k} \cdot \mathbf{B}_0 > 0$ and $\sigma_{\perp} \simeq -1$ for $\mathbf{k} \cdot \mathbf{B}_0 < 0$ (Gary 1986; Howes & Quataert 2010). We calculate the median $k_{\perp} \rho_p$ at the peak value of σ_{\perp} from Figure 3 (not shown here) to assess the scale at which these fluctuations exist, finding that $k_{\perp} \rho_p \gtrsim 1$ where σ_{\perp} is largest in this space. Therefore, Figure 3 is consistent with the presence of outward propagating right-handed fluctuations (Case I from Table 1) that we interpret as KAW-like fluctuations from the turbulent cascade. The peak $|\sigma_{\perp}| < 1$ is consistent with the nonlinear nature of these fluctuations.

5. Conclusions

We use a novel analysis technique to recover information about the wave-vector of solar wind fluctuations using single-point spacecraft measurements. We separate the contributions to magnetic helicity into two components with respect to \mathbf{B}_0 : one for fluctuations propagating at quasi-parallel angles and the other for those propagating at oblique angles. We analyze over 1.6 million magnetic field and ion spectra from the *Wind* MFI and SWE instruments and quantify the amplitude of the helicity contributions $\sigma_{||}$ and σ_{\perp} to explore the sources of fluctuations at proton-kinetic scales.

By plotting the median $\sigma_{||}$ -value across $\beta_{p,||} - T_{p,\perp}/T_{p,||}$ space, we show that there is a significant negative enhancement in $\sigma_{||}$ in unstable regions of both the AIC and parallel firehose instabilities. The median value of $\sigma_{||}$ reaches a minimum of

$\sigma_{\parallel} \simeq -0.6$ at $T_{p,\perp}/T_{p,\parallel} > 1$. In the spacecraft-frame, these quasi-parallel propagating fluctuations are left-handed, consistent with left-handed AIC waves propagating anti-sunward for $T_{p,\perp}/T_{p,\parallel} > 1$ and right-handed FMW waves propagating sunward in the plasma-frame for $T_{p,\perp}/T_{p,\parallel} < 1$. In regions of a negative enhancement in σ_{\parallel} , particularly for $T_{p,\perp}/T_{p,\parallel} > 1$, we also observe a substantial α -particle drift with respect to the proton flow, consistent with predictions (Podesta & Gary 2011a, 2011b). Elsewhere in $\beta_{p,\parallel} - T_{p,\perp}/T_{p,\parallel}$ space, $\sigma_{\parallel} \simeq 0$, which indicates no coherence in \mathbf{B} . This result suggests that fluctuations propagating quasi-parallel to \mathbf{B}_0 predominantly arise from ion instabilities, consistent with the background solar wind turbulence producing Alfvénic fluctuations with $k_{\perp} \gg k_{\parallel}$. These results show that instabilities are active and modes generated by them are common in the solar wind.

In addition, we show for the first time that σ_{\perp} is distributed throughout the entire parameter space occupied by the solar wind and peaks at $\sigma_{\perp} \simeq 0.3$. This peak occurs at $T_{p,\perp} \simeq T_{p,\parallel}$ and $\beta_{p,\parallel} \simeq 0.8$, which is strongest in a region of $\beta_{p,\parallel} - T_{p,\perp}/T_{p,\parallel}$ space dominated by fast wind, suggesting that these fluctuations are more Alfvénic. Since $\sigma_{\perp} > 0$ and shows little dependence on $\beta_{p,\parallel}$ and $T_{p,\perp}/T_{p,\parallel}$, this signature is consistent with anisotropic fluctuations from the turbulent cascade with significant k_{\perp} at proton-kinetic scales. While we interpret these fluctuations as KAW-like modes, we do not rule out that other nonlinear turbulent fluctuations or structures contribute to this helicity signal. We conjecture that these fluctuations are insensitive to proton temperature anisotropy and instability growth, in agreement with Klein & Howes (2015). Furthermore, since the unstable AIC and FMW modes do not appear to interact with the turbulent cascade, and there is no evidence of helicity from turbulent fluctuations with significant k_{\parallel} , we provide evidence for a very limited role of quasi-parallel propagating fluctuations in solar wind turbulence at proton-kinetic scales.

Our results provide evidence that the behavior of fluctuations at proton-kinetic scales is independent of the origin and macroscopic properties of the solar wind. For example, left-handed AIC modes are generated in both fast and slow wind streams, depending only on the local properties of the plasma such as proton temperature anisotropy and the presence of α -particle differential flow. In addition, we find no evidence of a parallel-propagating contribution to the helicity from the turbulence cascade at these scales in the stable parameter regime. Any Alfvénic fluctuations from the cascade with a significant k_{\parallel} would produce a signature in Figure 1 with a similar distribution to the right-handed signal in Figure 3. Therefore, we can rule out the existence of imbalanced fluctuations with $k_{\parallel} \gtrsim k_{\perp}$ that are not created by instabilities. This result constrains theories of turbulence in the solar wind and their implications for energy transport and dissipation.

The method we employ here can be applied to *Parker Solar Probe* and *Solar Orbiter* data to explore the role of fluctuations at kinetic scales in the corona and their evolution with increasing heliocentric distance. This will help us to diagnose the source and nature of the fluctuations that are crucial for the acceleration and heating of the solar wind.

We thank Kris Klein for useful scientific discussions and Mike Stevens for assistance with the SWE Faraday cup data.

Data from the *Wind* spacecraft are obtained from the SPDF website.¹⁰ L.D.W. is funded by an STFC Studentship; D.V. is supported by STFC Ernest Rutherford Fellowship ST/P003826/1; R.T.W. and C.J.O. are supported by the STFC consolidated grants to UCL/MSSL, ST/N000722/1 and ST/S000240/1. B.L.A. is supported by NASA grant 80NSSC18K0986.

ORCID iDs

Lloyd D. Woodham  <https://orcid.org/0000-0003-2845-4250>

Robert T. Wicks  <https://orcid.org/0000-0002-0622-5302>

Daniel Verscharen  <https://orcid.org/0000-0002-0497-1096>

Christopher J. Owen  <https://orcid.org/0000-0002-5982-4667>

Bennett A. Maruca  <https://orcid.org/0000-0002-2229-5618>

Benjamin L. Alterman  <https://orcid.org/0000-0001-6673-3432>

References

- Acuña, M. H., Ogilvie, K. W., Baker, D. N., et al. 1995, *SSRv*, 71, 5
- Alexandrova, O., Chen, C. H. K., Sorriso-Valvo, L., Horbury, T. S., & Bale, S. D. 2013, *SSRv*, 178, 101
- Alterman, B. L., Kasper, J. C., Stevens, M. L., & Koval, A. 2018, *ApJ*, 864, 112
- Bale, S. D., Kasper, J. C., Howes, G. G., et al. 2009, *PhRvL*, 103, 211101
- Bale, S. D., Kellogg, P. J., Mozer, F. S., Horbury, T. S., & Reme, H. 2005, *PhRvL*, 94, 215002
- Batchelor, G. K. 1970, *The Theory of Homogenous Turbulence* (Cambridge: Cambridge Univ. Press)
- Bourouaine, S., Verscharen, D., Chandran, B. D., Maruca, B. A., & Kasper, J. C. 2013, *ApJL*, 777, L3
- Bruno, R., & Carbone, V. 2013, *LRSF*, 10, 2
- Bruno, R., & Telloni, D. 2015, *ApJL*, 811, L17
- Chen, C. H. K. 2016, *JPIPh*, 82, 535820602
- Chen, C. H. K., Horbury, T. S., Schekochihin, A. A., et al. 2010, *PhRvL*, 104, 255002
- Chen, C. H. K., Klein, K. G., & Howes, G. G. 2019, *NatCo*, 10, 740
- Chen, C. H. K., Mallet, A., Schekochihin, A. A., et al. 2012, *ApJ*, 758, 120
- Chen, C. H. K., Mallet, A., Yousef, T. A., Schekochihin, A. A., & Horbury, T. S. 2011, *MNRAS*, 415, 3219
- Chew, G. F., Goldberger, M. L., & Low, F. E. 1956, *RSPSA*, 236, 112
- Gary, S. P. 1986, *JPIPh*, 35, 431
- Gary, S. P., Jian, L. K., Broiles, T. W., et al. 2015, *JGRA*, 121, 30
- He, J., Marsch, E., Tu, C. Y., Yao, S., & Tian, H. 2011, *ApJ*, 731, 85
- He, J., Tu, C. Y., Marsch, E., & Yao, S. 2012a, *ApJL*, 745, L8
- He, J., Tu, C. Y., Marsch, E., & Yao, S. 2012b, *ApJ*, 749, 86
- He, J., Wang, L., Tu, C. Y., Marsch, E., & Zong, Q. 2015, *ApJ*, 800, L31
- Hellinger, P., Trávníček, P. M., Kasper, J. C., & Lazarus, A. J. 2006, *GeoRL*, 33, L09101
- Horbury, T. S., Forman, M. A., & Oughton, S. 2008, *PhRvL*, 101, 175005
- Horbury, T. S., Wicks, R. T., & Chen, C. H. K. 2012, *SSRv*, 172, 325
- Howes, G. G., Dorland, W., Cowley, S. C., et al. 2008, *PhRvL*, 100, 065004
- Howes, G. G., & Quataert, E. 2010, *ApJL*, 709, L49
- Jian, L. K., Russell, C. T., Luhmann, J. G., et al. 2010, *JGRA*, 115, A12115
- Jian, L. K., Russell, C. T., Luhmann, J. G., et al. 2009, *ApJL*, 701, L105
- Jian, L. K., Wei, H. Y., Russell, C. T., et al. 2014, *ApJ*, 786, 123
- Kasper, J. C., Lazarus, A. J., & Gary, S. P. 2002, *GeoRL*, 29, 1839
- Kasper, J. C., Lazarus, A. J., & Gary, S. P. 2008, *PhRvL*, 101, 261103
- Kasper, J. C., Lazarus, A. J., Steinberg, J. T., Ogilvie, K. W., & Szabo, A. 2006, *JGRA*, 111, A03105
- Kasper, J. C., Maruca, B. A., Stevens, M. L., & Zaslavsky, A. 2013, *PhRvL*, 110, 091102
- Kasper, J. C., Klein, K. G., Weber, T., et al. 2017, *ApJ*, 849, 126
- Klein, K. G., Alterman, B. L., Stevens, M. L., Vech, D., & Kasper, J. C. 2018, *PhRvL*, 120, 205102
- Klein, K. G., & Howes, G. G. 2015, *PhPI*, 22, 032903

¹⁰ <http://spdf.gsfc.nasa.gov>

- Klein, K. G., Howes, G. G., TenBarge, J. M., & Podesta, J. J. 2014, *ApJ*, **785**, 138
- Koval, A., & Szabo, A. 2013, in AIP Conf. Proc. 1539, SOLAR WIND 13: Proceedings of the Thirteenth International Solar Wind Conference, ed. G. P. Zank et al. (Melville, NY: AIP), 211
- Lacombe, C., Alexandrova, O., & Matteini, L. 2017, *ApJ*, **848**, 45
- Leamon, R. J., Smith, C. W., Ness, N. F., & Wong, H. K. 1999, *JGRA*, **104**, 22331
- Lepping, R. P., Acuña, M. H., Burlaga, L. F., et al. 1995, *SSRv*, **71**, 207
- Markovskii, S. A., Vasquez, B. J., & Smith, C. W. 2015, *ApJ*, **806**, 78
- Marsch, E. 2012, *SSRv*, **172**, 23
- Maruca, B. A., Bale, S. D., Sorriso-Valvo, L., Kasper, J. C., & Stevens, M. L. 2013, *PhRvL*, **111**, 241101
- Maruca, B. A., Kasper, J. C., & Gary, S. P. 2012, *ApJ*, **748**, 137
- Matteini, L., Landi, S., Hellinger, P., et al. 2007, *GeoRL*, **34**, L20105
- Matthaeus, W. H., & Goldstein, M. L. 1982, *JGR*, **87**, 10347
- Matthaeus, W. H., Goldstein, M. L., & Smith, C. W. 1982, *PhRvL*, **48**, 1256
- Montgomery, M. D., & Turner, L. 1981, *PhFl*, **24**, 825
- Neugebauer, M., Goldstein, B. E., Bame, S. J., & Feldman, W. C. 1994, *JGRA*, **99**, 2505
- Neugebauer, M., Goldstein, B. E., Smith, E. J., & Feldman, W. C. 1996, *JGR*, **101**, 17047
- Ogilvie, K. W., Chornay, D. J., Fritzenreiter, R. J., et al. 1995, *SSRv*, **71**, 55
- Podesta, J. J., & Gary, S. P. 2011a, *ApJ*, **742**, 41
- Podesta, J. J., & Gary, S. P. 2011b, *ApJ*, **734**, 15
- Sahraoui, F., Goldstein, M. L., Belmont, G., Canu, P., & Rezeau, L. 2010, *PhRvL*, **105**, 131101
- Stansby, D., Horbury, T. S., & Matteini, L. 2019, *MNRAS*, **482**, 1706
- Steinberg, J. T., Lazarus, A. J., Ogilvie, K. W., Lepping, R. P., & Byrnes, J. B. 1996, *GeoRL*, **23**, 1183
- Taylor, G. I. 1938, *RSPSA*, **164**, 476
- Telloni, D., & Bruno, R. 2016, *MNRAS*, **463**, L79
- Telloni, D., Bruno, R., & Trenchi, L. 2015, *ApJ*, **805**, 46
- Torrence, C., & Compo, G. P. 1998, *BAMS*, **79**, 61
- Tsurutani, B. T., Arballo, J. K., Mok, J., et al. 1994, *GeoRL*, **21**, 633
- Verscharen, D., Bourouaine, S., & Chandran, B. D. 2013, *ApJ*, **773**, 163
- Verscharen, D., Klein, K. G., & Maruca, B. A. 2019, LRSP, in press (arXiv:1902.03448)
- Wicks, R. T., Forman, M. A., Horbury, T. S., & Oughton, S. 2012, *ApJ*, **746**, 103
- Wicks, R. T., Horbury, T. S., Chen, C. H. K., & Schekochihin, A. A. 2010, *MNRAS*, **407**, L31
- Wicks, R. T., Alexander, R. L., Stevens, M. L., et al. 2016, *ApJ*, **819**, 6
- Woodham, L. D., Wicks, R. T., Verscharen, D., & Owen, C. J. 2018, *ApJ*, **856**, 49
- Zhao, G. Q., Feng, H. Q., Wu, D. J., et al. 2018, *JGRA*, **123**, 1715
- Zhao, G. Q., Feng, H. Q., Wu, D. J., Pi, G., & Huang, J. 2019, *ApJ*, **871**, 175